crystals

MDPI

Article

Crystal Chemistry of Zinc Quinaldinate Complexes with Pyridine-Based Ligands

Barbara Modec

Department of Chemistry and Chemical Technology, University of Ljubljana; Večna pot 113, 1000 Ljubljana, Slovenia; barbara.modec@fkkt.uni-lj.si; Tel.: +386-1-4798-526

Received: 1 December 2017; Accepted: 16 January 2018; Published: 19 January 2018

Abstract: Substitution of methanol in $[Zn(quin)_2(CH_3OH)_2]$ ($quin^-$ denotes an anionic form of quinoline-2-carboxylic acid, also known as quinaldinic acid) with pyridine (Py) or its substituted derivatives, 3,5-lutidine (3,5-Lut), nicotinamide (Nia), 3-hydroxypyridine (3-Py-OH), 3-hydroxymethylpyridine (3-Hmpy), 4-hydroxypyridine (4-Py-OH) and 4-hydroxymethylpyridine (4-Hmpy), afforded a series of novel heteroleptic complexes with compositions $[Zn(quin)_2(Py)_2]$ (**1**), $[Zn(quin)_2(3,5\text{-}Lut)_2]$ (**2**), $[Zn(quin)_2(Nia)_2]\cdot 2CH_3CN$ (**3**), $[Zn(quin)_2(3\text{-}Py\text{-}OH)_2]$ (**4**), $[Zn(quin)_2(3\text{-}Hmpy)_2]$ (**5**), [Zn(quin)$_2$(4-Pyridone)] (**6**) (4-Pyridone = a keto tautomer of 4-hydroxypyridine), and $[Zn(quin)_2(4\text{-}Hmpy)_2]$ (**7**). In all reactions, the $\{Zn(quin)_2\}$ structural fragment with quinaldinate ions bound in a bidentate chelating manner retained its structural integrity. With the exception of [Zn(quin)$_2$(4-Pyridone)] (**6**), all complexes feature a six-numbered coordination environment of metal ion that may be described as a distorted octahedron. The arrangement of ligands is *trans*. The coordination sphere of zinc(II) in the 4-pyridone complex consists of only three ligands, two quinaldinates, and one secondary ligand. The metal ion thereby attains a five-numbered coordination environment that is best described as a distorted square-pyramid (τ parameter equals 0.39). The influence of substituents on the pyridine-based ligand over intermolecular interactions in the solid state is investigated. Since pyridine and 3,5-lutidine are not able to form hydrogen-bonding interactions, the solid state structures of their complexes, $[Zn(quin)_2(Py)_2]$ (**1**) and $[Zn(quin)_2(3,5\text{-}Lut)_2]$ (**2**), are governed by $\pi\cdots\pi$ stacking, C–H$\cdots\pi$, and C–H$\cdots$O intermolecular interactions. With other pyridine ligands possessing amide or hydroxyl functional groups, the connectivity patterns in the crystal structures of their complexes are governed by hydrogen bonding interactions. Thermal decomposition studies of novel complexes have shown the formation of zinc oxide as the end product.

Keywords: zinc(II) complexes; quinaldinic acid; pyridine; hydroxyl group; crystal structure; hydrogen bond

1. Introduction

The main interest in coordination chemistry of zinc finds its origin in its biological importance. In 1940, carbonic anhydrase II was discovered by Keilin and Mann as the first zinc-containing metalloenzyme [1]. The enzyme plays a key role in the transformation of carbon dioxide into bicarbonate in blood or in the reverse reaction in lungs. Since then, over 1000 zinc metalloenzymes, covering all classes of enzymes, have been discovered [2–6]. The prevalent use of zinc in biological systems is due to its unique properties [3,5,7–14]. Zinc(II) ion is characterized by a filled *d* subshell. Because of the latter, it lacks any redox activity which makes it an ideal metal cofactor for reactions that require a redox-stable center. The function of the ion is structural or that of a Lewis acid-type catalyst [15]. Since it does not act consistently either as a soft or as a hard Lewis acid, it presents a borderline case with no strong preference for coordination of either oxygen-, nitrogen- or sulfur-donor

ligands [16]. Another important property, which is again a direct consequence of the filled *d* subshell, is its ligand-field stabilization energy which is zero in all coordination environments [17]. Although no geometry is inherently more stable than another, the structurally characterized zinc enzymes display in most cases a distorted tetrahedral coordination environment of the metal ion [18,19]. Studies of synthetic analogues of enzymes, i.e., model compounds, could help in understanding how the immediate environment of the metal ion in an enzyme modulates its chemistry [20–22].

Quinaldinic acid (IUPAC name: quinoline-2-carboxylic acid), shown in Scheme 1, is a structural analogue of pyridine-2-carboxylic acid (known also as picolinic acid) which has found a wide use in the coordination chemistry of many transition metals. Upon giving off their protons, both acids form anions which possess two functional groups, a quinoline/pyridine nitrogen and a carboxylate, that can bind to transition metal cations. Although the recent literature abounds with structural data on picolinate complexes [23–27], the quinaldinate complexes remain relatively rare [28–32]. The quinaldinate ion can coordinate to metal ions in several ways (Scheme 2). A recent survey of the structurally characterized zinc(II) complexes with quinaldinate produced altogether six hits [33]. In all, the quinaldinate ion adopts the *N*,*O*-chelating binding mode through nitrogen and carboxylate oxygen, depicted as **a** in Scheme 2 and labelled as 1.101 in Harris notation [34]. One of the complexes, $[Zn(quin)_2(CH_3OH)_2]$ [35], was chosen for its labile methanol ligands to serve as an entry into the coordination chemistry of heteroleptic complexes that would contain apart from quinaldinate also a pyridine-based ligand. The pyridine ligands, used in this study (shown in Scheme 3), differ in the nature of their substituents and their relative positions on the ring. The ability of chosen ligands to participate in hydrogen-bonding is markedly different. The pyridine ligand is thus expected to have a crucial impact over strength and directionality of intermolecular interactions among complex molecules in solid state structures. Herein, we present the syntheses and the crystal structures of a series of zinc(II) complexes with quinaldinate and pyridine-based ligands. Reactions of methanol complex with pyridine-based ligands afforded $[Zn(quin)_2(Py)_2]$ (**1**), $[Zn(quin)_2(3,5\text{-}Lut)_2]$ (**2**), $[Zn(quin)_2(Nia)_2]\cdot 2CH_3CN$ (**3**), $[Zn(quin)_2(3\text{-}Py\text{-}OH)_2]$ (**4**), $[Zn(quin)_2(3\text{-}Hmpy)_2]$ (**5**), $[Zn(quin)_2(4\text{-}Pyridone)]$ (**6**), and $[Zn(quin)_2(4\text{-}Hmpy)_2]$ (**7**).

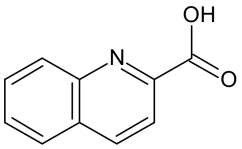

Scheme 1. Structural formula of quinaldinic acid.

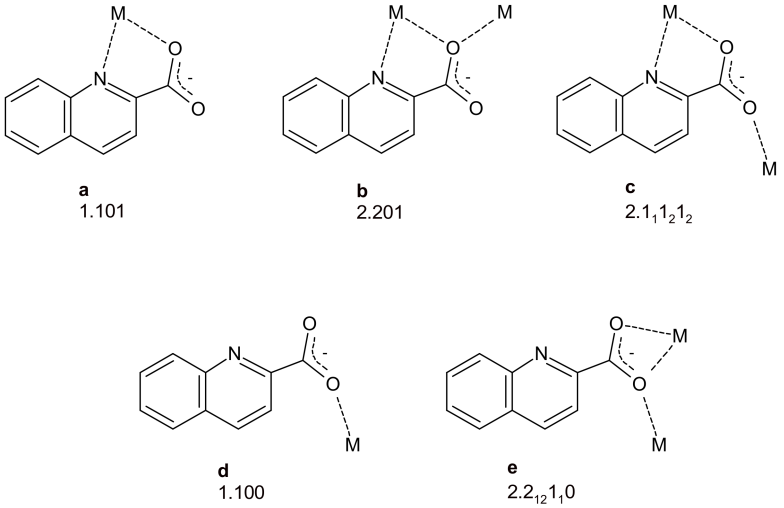

Scheme 2. Various coordination modes of quinaldinate, labelled following the Harris notation [33].

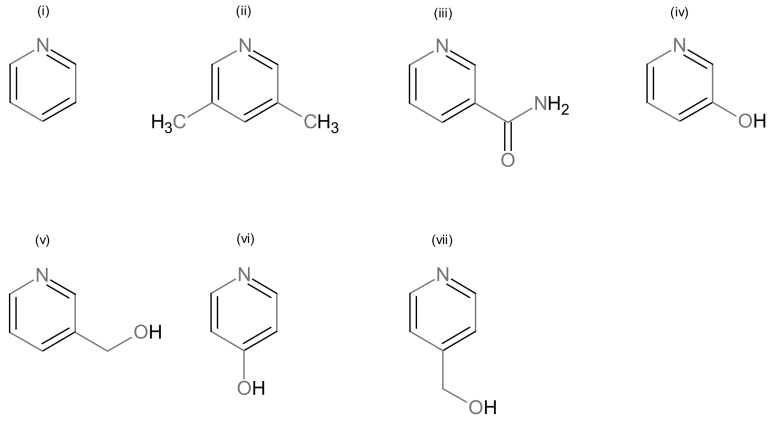

Scheme 3. Pyridine ligands, used in this work: (**i**) pyridine (Py), (**ii**) 3,5-lutidine (3,5-Lut), (**iii**) nicotinamide (Nia), (**iv**) 3-hydroxypyridine (3-Py-OH), (**v**) 3-hydroxymethylpyridine (3-Hmpy), (**vi**) 4-hydroxypyridine (4-Py-OH), and (**vii**) 4-hydroxymethylpyridine (4-Hmpy).

2. Materials and Methods

2.1. General

All manipulations and procedures were conducted in air. With the exception of acetonitrile, chemicals were purchased from Sigma Aldrich (St. Louis, MO, USA) and used as received. Acetonitrile was dried over molecular sieves, following the published procedure [36]. The IR spectra were measured on solid samples using a Perkin Elmer Spectrum 100 series FT-IR spectrometer (PerkinElmer, Shelton, CT, USA), equipped with ATR. Elemental analyses were performed by the Chemistry Department service at the University of Ljubljana. ^{1}H NMR spectra of DMSO-d_6 solutions were recorded on Bruker Avance DPX 300 MHz and/or Bruker Avance III 500 MHz NMR instruments (Bruker BioSpin GmbH, Rheinstetten, Germany). The chemical shifts (δ) were referenced to tetramethylsilane. The choice of dimethyl sulfoxide (DMSO) as a solvent was governed by a meagre solubility of complexes in other solvents. Upon dissolving, a substitution of pyridine-based ligands with DMSO molecules in the zinc(II) coordination sphere took place in all cases. From the solutions in NMR tubes, a complex of zinc(II) with DMSO crystallized as large, block-like crystals of a light yellow color. Their cell dimensions were the same as those of the known compound, $[Zn(quin)_2(DMSO)_2]\cdot 2DMSO$ [37]. The NMR spectra of compounds are thus the spectra of the DMSO complex and *free* pyridine-based ligands. Two representative spectra are given in Supplementary Materials. Thermal analyses were performed on a Mettler Toledo TG/DSC 1 instrument (Mettler Toledo, Schwerzenbach, Switzerland) in argon or air atmosphere at a 50 mL/min gas flow. Masses of the samples were in the 4–32 mg range. Samples in platinum crucibles were heated from room temperature to 800 °C with a heating rate of 5 K/min. In each case, the baseline was subtracted. The solid residue, a mixture of grey amorphous material and zinc oxide (zincite modification), was identified by X-ray powder diffraction (XRPD). XRPD data were collected with a PANalytical X'Pert PRO MD diffractometer (PANALYTICAL, Almelo, The Netherlands) by using Cu-Kα radiation (λ = 1.5406 Å).

2.2. Preparation Procedures

Preparation of $[Zn(quin)_2(CH_3OH)_2]$. A teflon container was loaded with zinc(II) acetate dihydrate (110 mg, 0.50 mmol) and quinaldinic acid (173 mg, 1.00 mmol). Methanol (15 mL) was added. The container was closed and inserted into a steel autoclave. The autoclave was heated for 24 h at 105 °C. The reaction vessel was then allowed to cool slowly to room temperature. Large colorless crystals of $[Zn(quin)_2(CH_3OH)_2]$ were collected by filtration. The mass of the dried product was 100 mg. Yield: 0.21 mmol, 42%. Note. The crystals were found to lose their lustre after a prolonged period.

Preparation of [Zn(quin)$_2$(Py)$_2$] (**1**). A teflon container was loaded with [Zn(quin)$_2$(CH$_3$OH)$_2$] (50 mg, 0.11 mmol), pyridine (2 mL), and dried acetonitrile (7.5 mL). The container was closed and inserted into a steel autoclave. The autoclave was heated for 24 h at 105 °C. The reaction vessel was then allowed to cool slowly to room temperature. Large colorless crystals of **1** were collected by filtration. The mass of the dried product was 41 mg. Yield: 0.072 mmol, 66%. Found C, 63.16; H, 3.86; N, 9.84%. $C_{30}H_{22}N_4O_4Zn$ requires C, 63.45; H, 3.90; N, 9.87%. IR (ATR, cm^{-1}): 3069w, 1647vvs [ν_{asym}(COO)], 1594s, 1566s, 1508m, 1484m, 1467m, 1440vs, 1362vvs, 1351vvs [ν_{sym}(COO)], 1292w, 1270m, 1209m, 1176m, 1159m, 1149m, 1111w, 1071m, 1036m, 1005m, 959m, 891s, 856s, 802vvs, 771vvs, 759vvs, 744s, 703vvs, 636s, 620s. ^{1}H NMR (DMSO) δ/ppm: 7.39 (m, 2H), 7.76–7.85 (m, 1H), 8.58 (m, 2H) [pyridine signals]; 7.76–7.85 (m, 1H), 8.11 (m, 1H), 8.20 (d, J = 7.9 Hz, 1H), 8.41 (d, J = 8.5 Hz, 1H), 8.80 (m, 2H) [quinaldinate signals].

Preparation of [Zn(quin)$_2$(3,5-Lut)$_2$] (**2**). A teflon container was loaded with [Zn(quin)$_2$(CH$_3$OH)$_2$] (50 mg, 0.11 mmol), 3,5-lutidine (1 mL), and dried acetonitrile (10 mL). The container was closed and inserted into a steel autoclave. The autoclave was heated for 24 h at 105 °C. The reaction vessel was then allowed to cool slowly to room temperature. Large, light yellow crystals of **2** were collected by filtration. The mass of the dried product was 55 mg. Yield: 0.088 mmol, 80%. Found C, 65.30; H, 4.52; N, 9.02%. $C_{34}H_{30}N_4O_4Zn$ requires C, 65.44; H, 4.85; N, 8.98%. IR (ATR, cm^{-1}): 3113w, 3066w, 2912w, 1654vvs [ν_{asym}(COO)], 1593s, 1564m, 1551m, 1507m, 1458s, 1428m, 1405w, 1355vvs [ν_{sym}(COO)], 1343vs, 1320s, 1294w, 1269m, 1243w, 1215w, 1205w, 1172s, 1147vs, 1115m, 1034w, 1023w, 1000w, 986w, 957s, 940w, 893s, 870s, 861s, 811s, 800vs, 772vvs, 743vs, 706vvs, 635vs. ^{1}H NMR (DMSO) δ/ppm: 2.25 (s, 6H), 7.42 (s, 1 H), 8.19 (s, 2H) [3,5-lutidine signals]; 7.82 (m, 1H), 8.01 (m, 1H), 8.19 (d, J = 7.9 Hz, 1H), 8.41 (d, J = 8.4 Hz, 1H), 8.78 (m, 2H) [quinaldinate signals].

Preparation of [Zn(quin)$_2$(Nia)$_2$]·2CH$_3$CN (**3**). A teflon container was loaded with [Zn(quin)$_2$(CH$_3$OH)$_2$] (50 mg, 0.11 mmol), nicotinamide (120 mg, 0.98 mmol) and dried acetonitrile (10 mL). The container was closed and inserted into a steel autoclave. The autoclave was heated for 24 h at 105 °C. The reaction vessel was then allowed to cool slowly to room temperature. A colorless microcrystalline solid was collected by filtration. Mass of the dried product was 47 mg. Yield: 0.072 mmol, 65%. Note. The crystals lost interstitial solvent upon removal from mother liquor. Found C, 58.28; H, 3.61; N, 12.47%. $C_{32}H_{24}N_6O_6Zn$ (complex without acetonitrile solvent) requires C, 58.77; H, 3.70; N, 12.85%. IR (ATR, cm^{-1}): 3292m, 3147m [ν(N–H), amide], 2256w [ν(CN), acetonitrile], 1692s [ν(C=O), amide], 1676w, 1651w, 1624vvs [ν_{asym}(COO)], 1600vvs, 1565m, 1506w, 1479w, 1459s, 1432m, 1383m, 1363vvs [ν_{sym}(COO)], 1342s, 1330m, 1263w, 1250w, 1217w, 1203m, 1168s, 1159m, 1147s, 1114w, 1059s, 1041w, 1020w, 992w, 957m, 945m, 922w, 897s, 880m, 856s, 807vs, 775vvs, 743m, 695vvs, 670m, 653vs, 632s. ^{1}H NMR (DMSO) δ/ppm: 7.50 (m, 1H), 7.58 (br, 1H), 8.14 (br, 1H), 8.22 (m, 1H), 8.70 (dd, 1H), 9.03 (dd, 1H) [nicotinamide signals]; 7.82(m, 1H), 8.01 (m, 1H), 8.22 (d, J = 7.9 Hz, 1H), 8.41 (d, J = 8.4 Hz, 1H), 8.80 (m, 2H) [quinaldinate signals]; 2.08 (s, 3H) [methyl, acetonitrile].

Preparation of [Zn(quin)$_2$(3-Py-OH)$_2$] (**4**). A teflon container was loaded with [Zn(quin)$_2$(CH$_3$OH)$_2$] (50 mg, 0.11 mmol), 3-hydroxypyridine (150 mg, 1.58 mmol), and dried acetonitrile (10 mL). The container was closed and inserted into a steel autoclave. The autoclave was heated for 24 h at 105 °C. The reaction vessel was then allowed to cool slowly to room temperature. The solid consisted mostly of the unreacted ligand (large orange-colored crystals), [Zn(quin)$_2$(H$_2$O)] (colorless, crystalline solid) and [Zn(quin)$_2$(3-Py-OH)$_2$] (**4**) (a few block-like colorless crystals). The identity of the orange crystalline material was determined by its infrared spectrum and ^{1}H NMR which were identical to the spectra of pure ligand. The aqua complex was identified by its infrared spectrum. Repeated attempts to improve the yield were not met with success.

Preparation of [Zn(quin)$_2$(3-Hmpy)$_2$] (**5**). A teflon container was loaded with [Zn(quin)$_2$(CH$_3$OH)$_2$] (50 mg, 0.11 mmol), 3-hydroxymethylpyridine (1.5 mL), and dried acetonitrile (10 mL). The container was closed and inserted into a steel autoclave. The autoclave was heated for 24 h at 105 °C. The

reaction vessel was then allowed to cool slowly to room temperature. Large block-like crystals of **5** of a gold yellow color were collected by filtration. Mass of the dried product was 43 mg. Yield: 0.068 mmol, 62%. Found C, 61.27; H, 4.10; N, 9.16%. $C_{32}H_{26}N_4O_6Zn$ requires C, 61.20; H, 4.17; N, 8.92%. IR (ATR, cm^{-1}): 3367s [ν(O–H), 3-Hmpy], 3071w, 2824w, 1638vvs [ν_{asym}(COO)], 1597vs, 1581m, 1566m, 1554m, 1506m, 1479w, 1460s, 1428vs, 1368vvs [ν_{sym}(COO)], 1348m, 1336m, 1305s, 1273m 1234w, 1204s, 1191m, 1177m, 1152s, 1128w, 1107w, 1062vvs, 1048vs [ν(C–O), 3-Hmpy], 1031m, 1010w, 968m, 926w, 897s, 858s, 796vvs, 775vvs, 708vvs, 646m, 633vs. ^{1}H NMR (DMSO) δ/ppm: 4.53 (d, J = 5.6 Hz, 2H), 5.35 (t, J = 5.7 Hz, 1H), 7.37 (m, 1H), 7.73 (d, J = 7.8 Hz, 1H), 8.46 (d, J = 3.7 Hz, 1H), 8.53 (d, J = 1 Hz, 1H) [3-hydroxymethylpyridine signals]; 7.81 (m, 1H), 7.93 (m, 1H), 8.20 (d, J = 8.0 Hz, 1H), 8.43 (d, J = 8.4 Hz, 1H), 8.80 (m, 2H) [quinaldinate signals].

Preparation of [Zn(quin)$_2$(4-Pyridone)] (**6**). A teflon container was loaded with [Zn(quin)$_2$(CH_3OH)$_2$] (50 mg, 0.11 mmol), 4-hydroxypyridine (110 mg, w = 0.95, 1.10 mmol), triethylamine (250 mg, 2.47 mmol), and dried acetonitrile (10 mL). The container was closed and inserted into a steel autoclave. The autoclave was heated for 24 h at 105 °C. The reaction vessel was then allowed to cool slowly to room temperature. Block-like crystals of **6** of a gold yellow color were collected by filtration. The mass of the dried product was 32 mg. Yield: 0.063 mmol, 57%. Found C, 59.01; H, 3.70; N, 8.39%. $C_{25}H_{17}N_3O_5Zn$ requires C, 59.48; H, 3.39; N, 8.32%. IR (ATR, cm^{-1}): 3077w, 1644vvs [ν_{asym}(COO)], 1603vvs, 1570m, 1530vvs, 1462vs, 1367vvs [ν_{sym}(COO)], 1264m, 1201s, 1177s, 1151m, 1115w, 1049s, 1017vvs [ν(C–O), 4-pyridone], 965m, 900m, 872w, 848vvs, 804vvs, 775vvs, 739m, 639s, 606s. ^{1}H NMR (DMSO) δ/ppm: 6.13 (d, J = 6.6 Hz, 2H), 7.61 (d, J = 5.0 Hz, 2H) [4-pyridone signals]; 7.77 (m, 2H), 7.87 (m, 2H), 8.17 (d, J = 8.1 Hz, 2H), 8.35 (d, J = 8.4 Hz, 2H), 8.47 (d, J = 8.2 Hz, 2H), 8.76 (d, J = 8.3 Hz, 2H) [quinaldinate signals].

Preparation of [Zn(quin)$_2$(4-Hmpy)$_2$] (**7**). A teflon container was loaded with [Zn(quin)$_2$(CH_3OH)$_2$] (50 mg, 0.11 mmol), 4-hydroxymethylpyridine (110 mg, 1.00 mmol), and dried acetonitrile (15 mL). The container was closed and inserted into a steel autoclave. The autoclave was heated for 24 h at 105 °C. The reaction vessel was then allowed to cool slowly to room temperature. Large block-like crystals of **7** of a gold yellow color were collected by filtration. The mass of the dried product was 36 mg. Yield: 0.057 mmol, 52%. Found C, 61.21; H, 4.06; N, 8.89%. $C_{32}H_{26}N_4O_6Zn$ requires C, 61.20; H, 4.17; N, 8.92%. IR (ATR, cm^{-1}): 3287m [ν(O–H), 4-Hmpy], 3076w, 2832w, 1632vvs [ν_{asym}(COO)], 1602s, 1565m, 1555s, 1505m, 1458s, 1418s, 1367vvs [ν_{sym}(COO)], 1343vs, 1318s, 1270m, 1235w, 1215s, 1204m, 1176s, 1148m, 1114w, 1095s, 1067vs, 1022w, 1010vs [ν(C–O), 4-Hmpy], 996m, 963s, 897vs, 854vs, 802vvs, 779vvs, 720m, 687s, 665w, 637vs. ^{1}H NMR (DMSO) δ/ppm: 4.53 (d, J = 5.6 Hz, 2H), 5.40 (t, J = 5.7 Hz, 1H), 7.31 (d, J = 5.8 Hz, 2H), 8.41 (d, J = 5.9 Hz, 2H) [4-hydroxymethylpyridine signals]; 7.82 (m, 1H), 8.00 (m, 1H), 8.20 (d, J = 8.1 Hz, 1H), 8.41 (d, J = 8.4 Hz, 1H), 8.80 (m, 2H) [quinaldinate signals].

2.3. X-ray Structure Determinations

Each crystal was mounted on the tip of a glass fiber with a small amount of silicon grease and transferred to a goniometer head. Data were collected on an Agilent SuperNova diffractometer (Agilent Technologies XRD Products, Oxfordshire, UK), using graphite-monochromatized Mo-Kα radiation at 150 K. Data reduction and integration were performed with the software package CrysAlis PRO [38]. Corrections for the absorption (multi-scan) were made in all cases. The coordinates of the majority of non-hydrogen atoms were found via direct methods using the structure solution program SHELXS [39]. The positions of the remaining non-hydrogen atoms were located by use of a combination of least-squares refinement and difference Fourier maps in the SHELXL-97 program [40]. The positions of NH, NH_2, and OH hydrogen atoms in **3**–**7** were unambiguously located from the residual electron density maps. All other hydrogen atoms were placed in geometrically calculated positions and refined using a riding model. A summary of crystal data and refinement parameters for **1**–**7** is given in Table 1. Figures depicting the structures were prepared by ORTEP3 [41], Mercury [42], and CrystalMaker [43].

Table 1. Crystallographic data for **1**–**7**.

	1	**2**	**3**	**4**	**5**	**6**	**7**
Empirical formula	$C_{30}H_{22}N_4O_4Zn$	$C_{34}H_{30}N_4O_4Zn$	$C_{36}H_{30}N_8O_6Zn$	$C_{30}H_{22}N_4O_6Zn$	$C_{32}H_{26}N_4O_6Zn$	$C_{25}H_{17}N_3O_5Zn$	$C_{32}H_{26}N_4O_6Zn$
Formula weight	567.89	623.99	736.05	599.89	627.94	504.79	627.94
Crystal system	monoclinic	triclinic	monoclinic	monoclinic	triclinic	monoclinic	monoclinic
Space group	$P\,2_1/c$	$P\,-1$	$P\,2_1/n$	$P\,2_1/n$	$P\,-1$	$P\,2_1/n$	$P\,2_1/n$
T [K]	150(2)	150(2)	150(2)	150(2)	150(2)	150(2)	150(2)
a [Å]	8.8768(11)	8.0866(4)	8.7982(4)	9.8119(5)	7.1034(4)	11.2818(4)	8.8653(6)
b [Å]	9.5542(17)	9.2741(3)	14.0204(5)	9.6039(4)	9.6254(5)	15.0187(6)	17.9746(10)
c [Å]	15.592(2)	9.9121(4)	14.3149(7)	13.8912(9)	10.7604(6)	13.3256(6)	9.6797(6)
α [°]	90	96.315(3)	90	90	97.779(5)	90	90
β [°]	105.972(13)	96.506(4)	105.608(5)	102.700(6)	109.171(5)	101.321(4)	116.307(8)
γ [°]	90	100.997(3)	90	90	99.391(4)	90	90
V [Å^3]	1271.3(3)	718.39(5)	1700.69(13)	1276.98(12)	671.37(6)	2213.93(15)	1382.71(15)
D_{calcd} [g/cm^3]	1.484	1.442	1.437	1.56	1.553	1.153	1.508
Z	2	1	2	2	1	4	2
λ [Å]	0.71073	0.71073	0.71073	0.71073	0.71073	0.71073	0.71073
μ [mm^{-1}]	1.011	0.902	0.781	1.017	0.971	1.153	0.943
Collected reflections	6568	6544	10541	7407	5739	12358	6568
Unique reflections, R_{int}	2899, 0.0839	3309, 0.0287	3907, 0.0490	2886, 0.0349	3077, 0.0304	5082, 0.0320	3179, 0.0267
Observed reflections	1931	3054	2849	2245	2788	4254	2621
$R1$ [1] ($I > 2\sigma(I)$)	0.052	0.0379	0.0409	0.034	0.0364	0.0325	0.0302
$wR2$ [2] (all data)	0.1206	0.097	0.0915	0.075	0.0878	0.0801	0.0748

[1] $R1 = \sum | |F_o| - |F_c| | / \sum |F_o|$. [2] $wR2 = \{\sum[w(F_o^2 - F_c^2)^2] / \sum[w(F_o^2)^2]\}^{1/2}$.

3. Results and Discussion

3.1. Synthetic Aspects

A straightforward synthesis of heteroleptic Zn(II) complexes with quinaldinate and a secondary pyridine ligand was based on a facile substitution of labile methanol ligands in $[Zn(quin)_2(CH_3OH)_2]$. The $\{Zn(quin)_2\}$ core with quinaldinates bound in a chelating manner was not expected to undergo any significant structural changes. With the exception of the hydroxypyridine ligands, the proposed strategy resulted in novel complexes in reasonable yields. An excess of pyridine ligand was required to avoid the coordination of water to the zinc ion. The amount of water remaining in the solvent after drying was sufficient for the formation of an aqua complex. The reaction outcomes of the 3- or 4-hydroxypyridine systems were not as anticipated. Hydroxypyridines are prone to enol-ketonic tautomerism which strongly affects their nature, including their ability to function as ligands [44,45]. For 4-hydroxypyridine, the keto form is a dominant one in the solid state. The product isolated from the 4-Py-OH reaction mixture is $[Zn(quin)_2(4\text{-Pyridone})]$ (**6**), a complex with pyridone. It is to be noted that for its isolation the reaction mixture had to contain a stoichiometric amount of triethylamine. In the absence of base, no complex of zinc(II) with any form of 4-Py-OH was obtained. Following literature examples [46,47], the amine should assist in deprotonation of hydroxypyridine with the resulting anionic species engaging both donor sites in coordination. In the case of 3-Py-OH, the ligand in the solid state is known to consist of a mixture of both the neutral and the bipolar forms connected by strong intermolecular hydrogen bonds [48]. The formation of zwitterionic species is associated mainly with the acid-base properties of 3-Py-OH. Upon the protonation of nitrogen, the ligand's tendency towards ligation of metal ions is highly diminished. A negligible yield of $[Zn(quin)_2(3\text{-Py-OH})_2]$ (**4**) speaks in favor of the zwitterion being a major contributor also in the reaction system described in this paper.

3.2. Description of Structures

The title zinc(II) quinaldinate complexes with pyridine ligands are neutral. The first coordination sphere of zinc(II) ion consists in all but a 4-pyridone complex **6** of two quinaldinates and two pyridine-based ligands in an all trans arrangement. The N_4O_2 donor set renders a distorted octahedral environment around the zinc(II) ion. Because of the similarity of complexes, their molecular structures will be described together. They crystallize in centrosymmetric space groups with zinc ions located on the inversion centers. The coordination molecules possess an inherent crystallographic symmetry which places them in C_i point group. In each case, the asymmetric unit consists of a half of a complex molecule. The Oak Ridge Thermal Ellipsoid Plot (ORTEP) drawings of $[Zn(quin)_2(Py)_2]$ (**1**), $[Zn(quin)_2(Nia)_2]\cdot 2CH_3CN$ (**3**), and $[Zn(quin)_2(3\text{-Py-OH})_2]$ (**4**) are shown in Figures 1–3, whereas the drawings of $[Zn(quin)_2(3,5\text{-Lut})_2]$ (**2**), $[Zn(quin)_2(3\text{-Hmpy})_2]$ (**5**), and $[Zn(quin)_2(4\text{-Hmpy})_2]$ (**7**) are given in the Supplementary Materials.

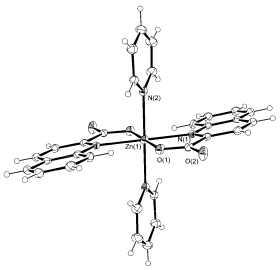

Figure 1. The ORTEP drawing of $[Zn(quin)_2(Py)_2]$ (**1**). Atoms are represented by displacement ellipsoids at the 30% probability level. Hydrogen atoms are shown as spheres of arbitrary radii. Selected bond lengths [Å] and angles [°]: Zn(1)–N(1) = 2.225(13), Zn(1)–O(1) = 2.0249(19), Zn(1)–N(2) = 2.214(2), O(1)–Zn(1)–N(1) = 79.52(9), O(1)–Zn(1)–N(2) = 90.81(8), N(1)–Zn(1)–N(2) = 93.76(10).

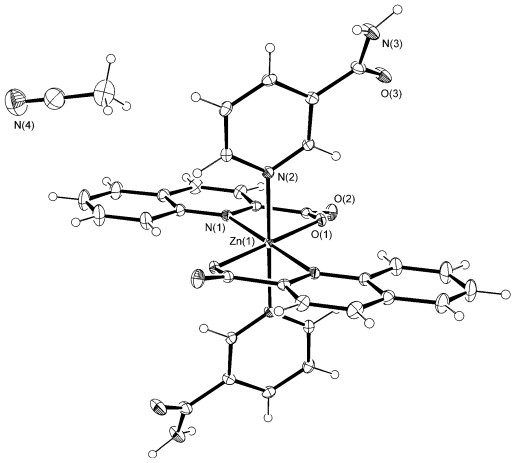

Figure 2. The ORTEP drawing of $[Zn(quin)_2(Nia)_2]\cdot 2CH_3CN$ (**3**). Atoms are represented by displacement ellipsoids at the 30% probability level. Hydrogen atoms are shown as spheres of arbitrary radii. Selected bond lengths [Å] and angles [°]: Zn(1)–N(1) = 2.2248(19), Zn(1)–O(1) = 2.0519(14), Zn(1)–N(2) = 2.1861(17), O(1)–Zn(1)–N(1) = 78.21(6), O(1)–Zn(1)–N(2) = 91.74(6), N(1)–Zn(1)–N(2) = 92.92(7).

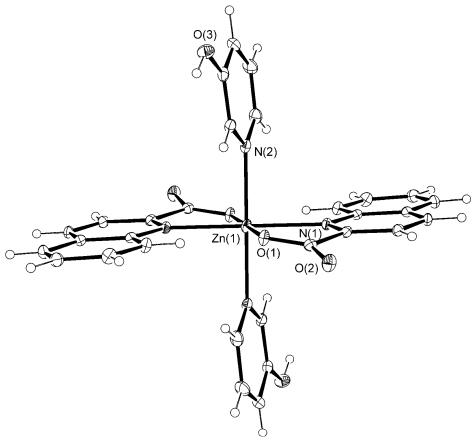

Figure 3. The ORTEP drawing of $[Zn(quin)_2(3\text{-Py-OH})_2]$ (**4**). Atoms are represented by displacement ellipsoids at the 30% probability level. Hydrogen atoms are shown as spheres of arbitrary radii. Selected bond lengths [Å] and angles [°]: Zn(1)–N(1) = 2.2298(15), Zn(1)–O(1) = 2.0391(13), Zn(1)–N(2) = 2.2008(17), O(1)–Zn(1)–N(1) = 78.86(5), O(1)–Zn(1)–N(2) = 91.36(6), N(1)–Zn(1)–N(2) = 90.44(6).

The relevant bonding parameters are summed up in Table 2. Pyridine-based ligands are coordinated via their nitrogen atoms. The pendant OH or CH_2OH groups of 3-Py-OH, 3-Hmpy, and 4-Hmpy ligands did not interact with zinc(II) ion. The zinc-to-pyridine ligand bond lengths span a somewhat wide range, 2.1861(17)–2.2420(14) Å, with the shortest ones occurring in the nicotinamide complex **3** and the 3-Hmpy complex **5** while the longest one occurs in the 4-Hmpy complex **7**. The quinaldinate has adopted its most common binding mode, the *N*,*O*-chelating coordination with the zinc-to-nitrogen bond lengths in the 2.2214(14)–2.2462(17) Å range and the zinc-to-oxygen bond lengths in the 2.0208(11)–2.0519(14) Å range. The series displays a pronounced similarity in the binding parameters. With a chelating quinaldinate coordination to zinc(II), a stable five-membered chelate ring is formed with bite angles in the 77.94(6)–79.52(9)° range. The chelate ring is not planar.

Table 2. Relevant bonding parameters [Å, °] of novel zinc(II) quinaldinate complexes.

Parameter	1	2	3	4	5	6	7
Zn–quin$^-$							
Zn–N	2.225(3)	2.2277(16)	2.2248(19)	2.2298(15)	2.2462(17)	2.1425(15) and 2.1496(15)	2.2214(14)
Zn–O	2.0249(19)	2.0147(14)	2.0519(14)	2.0391(13)	2.0500(13)	1.9952(13) and 2.0333(13)	2.0208(11)
bite angle	79.52(9)	78.66(6)	78.21(6)	78.86(5)	77.94(6)	79.85(6) and 79.23(5)	78.06(5)
torsion angle [1]	6.9(4)	4.1(3)	11.4(3)	13.6(3)	7.6(3)	6.1(2) and 6.0(2)	2.9(2)
dihedral angle [2]	8.5(5)	5.5(3)	11.6(4)	13.7(3)	7.0(3)	7.1(3) and 7.4(3)	2.7(3)
C–O	1.230(3), 1.269(4)	1.225(3), 1.273(2)	1.238(3), 1.270(3)	1.241(2), 1.263(2)	1.235(2), 1.264(3)	1.228(2), 1.282(2)	1.235(2), 1.271(2)
Zn–pyridine ligand							
L	Py	3,5-Lut	Nia	3-Py-OH	3-Hmpy	4-pyridone	4-Hmpy
donor atom	N	N	N	N	N	O	N
Zn–L	2.214(2)	2.2395(17)	2.1861(17)	2.2008(17)	2.1868(16)	1.9602(13)	2.2420(14)

[1] N–C(*ortho*)–C(carboxylate)–O(coordinated carboxylate oxygen). It gives the deviation from the planarity of the five-numbered chelate ring. [2] Defined as a dihedral angle between the plane of the quinaldinate ring and the carboxylate group.

Its non-planarity may be described by a torsion angle involving four of its atoms. The largest value, i.e., 13.6(3)°, calculated for 3-hydroxypyridine complex [Zn(quin)$_2$(3-Py-OH)$_2$] (**4**), corresponds to the least planar ring. As a consequence, the carboxylate functional group is not coplanar with the quinoline plane. Its non-coordinated or *free* oxygen atom points out from the aromatic plane. The disruption of planarity can be measured by a dihedral angle formed between the quinoline plane and the carboxylate plane. The largest value was observed again in the 3-Py-OH complex **4**, whereas the 4-Hmpy complex **7** shows the smallest deviation from planarity. A twist of carboxylate with respect to the quinoline ring was noted previously for a related compound, [Zn(quin)$_2$(1-methylimidazole)$_2$] [49]. The distortion was attributed to the involvement of *free* carboxylate oxygen in intermolecular interactions. As will be shown presently, the *free* carboxylate oxygen atoms in compounds **1**–**5** and **7** also participate in intermolecular interactions. For each complex in the homologous series, the extent of distortion was compared to the strength of intermolecular interactions. It turns out that obvious correlation exists only for [Zn(quin)$_2$(3-Py-OH)$_2$] (**4**) where the greatest deviation corresponds to the shortest and thus the strongest interaction, i.e., a hydrogen bond of the O–H···COO$^-$ type. Contrary to expectations, [Zn(quin)$_2$(Py)$_2$] (**1**), which lacks strong intermolecular interactions, still displays a non-negligible distortion.

The 4-Pyridone complex [Zn(quin)$_2$(4-Pyridone)] (**6**) differs from other members of the series. Its ORTEP drawing is presented in Figure 4. The first coordination sphere of zinc(II) consists of two quinaldinates and a single 4-pyridone ligand, rendering the N_2O_3 donor set. The pyridone ligand has coordinated to zinc(II) through the phenoxide oxygen atom. The molecule possesses no intrinsic crystallographic symmetry. The pair of quinaldinate ions, bound in the usual *N*,*O*-chelating manner with bite angles of 79.23(5) and 79.85(6)°, is no longer nearly coplanar as in the case of the other six complexes. In the absence of the fourth ligand, the quinaldinates bend away from the equatorial plane. The value of a dihedral angle between the quinaldinates amounts to 52.65(4)°. Furthermore, the zinc-to-quinaldinate bonds in **6** are significantly shorter than in the other six complexes. The orientation of pyridone is skewed with respect to the Zn–O vector, an angle of 136.40(6)° is formed between the latter and the O–N pyridone axis. The H···Zn distance is just below the 3.2 Å cut-off, the limit in considering the pseudo agostic H···M (M = transition metal cation) bonds [50,51]. Nevertheless, in complex **6** it is more the ligand structure that holds the C–H bond close to the metal than the attraction of C–H to the metal ion.

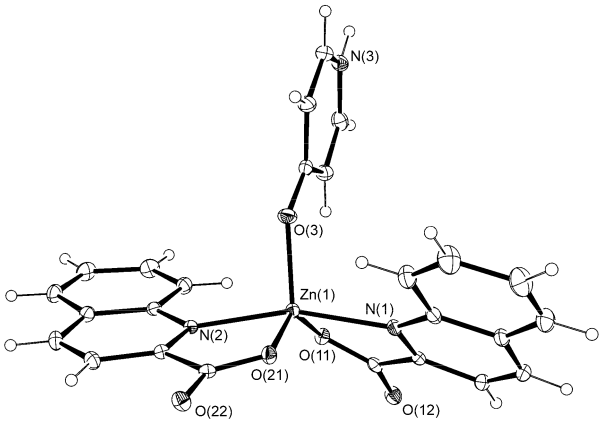

Figure 4. The ORTEP drawing of [Zn(quin)$_2$(4-Pyridone)] (**6**). Atoms are represented by displacement ellipsoids at the 30% probability level. Hydrogen atoms are shown as spheres of arbitrary radii. Selected bond lengths [Å] and angles [°]: Zn(1)–N(1) = 2.1425(15), Zn(1)–O(11) = 1.9952(13), Zn(1)–N(2) = 2.1496(15), Zn(1)–O(21) = 2.0333(13), Zn(1)–O(3) = 1.9602(13), O(11)–Zn(1)–N(1) = 79.85(6), O(21)–Zn(1)–N(2) = 79.23(5), O(21)–Zn(1)–O(11) = 138.17(5), N(2)–Zn(1)–N(1) = 161.26(6), O(3)–Zn(1)–N(1) = 100.45(6), O(3)–Zn(1)–O(11) = 115.49(6), O(3)–Zn(1)–N(2) = 96.84(6), O(3)–Zn(1)–O(21) = 106.13(5).

All known zinc(II) quinaldinate complexes possess quinaldinato ligands coordinated in the *N*,*O*-chelating fashion. Not only the composition but also the arrangement of ligands in three of these compounds is similar to compounds **1**–**5** and **7**: the mutual arrangement of ligands in $[Zn(quin)_2(1\text{-methylimidazole})_2]$ [49], $[Zn(quin)_2(CH_3OH)_2]$ [35], and $[Zn(quin)_2(DMSO)_2]\cdot 2DMSO$ [37] is *trans*. In contrast to the above examples, the arrangement of ligands in $[Zn(quin)_2(Him)_2]$, a complex with imidazole, is *cis* [52]. As can be seen from Tables 2 and 3, the zinc-to-quinaldinate bond lengths in our compounds are of similar lengths to the ones shown in the cited examples. The remaining two literature examples, [Zn(Mepa)(quin)] ($Mepa^-$ = the anionic form of N-(2-mercaptoethyl)picolylamine) [53] and $[Zn(quin)_2(H_2O)]$ [54], feature a five-numbered coordination environment of the metal. The arrangement of five donor atoms is intermediate between the square-pyramidal and trigonal-bipyramidal extremes. A degree of trigonality in five-coordinate systems is quantified by the geometric parameter, known as τ [55]. The value of 0.57 for $[Zn(quin)_2(H_2O)]$ suggests a slightly greater distortion away from the tetragonal than for $[Zn(quin)_2(4\text{-Pyridone})]$ (**6**) with the τ value of 0.39. An appropriate description of the coordination polyhedron of the 4-pyridone complex is thus that of a distorted square pyramid with pyridone oxygen located at the apical site. In **6**, the zinc(II) ion lies ca. 0.5 Å above the basal plane, defined by the quinaldinate donor atoms. The similarity of bonding parameters of 4-pyridone complex **6** and aqua complex is obvious. Both display significantly shorter bonds than complexes with six donor atoms. This adds validity to the rule that with a smaller number of ligands, the bonds in the immediate vicinity of the metal ion are shorter.

Table 3. Relevant bonding parameters [Å, °] of zinc complexes with quinaldinate, literature data.

Complex	Zn–N	Zn–O	Zn–L	Ref.
$[Zn(quin)_2(1\text{-methylimidazole})_2]$	2.244(2)	2.057(2)	2.144(2)	[49]
$[Zn(quin)_2(CH_3OH)_2]$	2.231(1)	2.003(1)	2.170(2)	[35]
cis-$[Zn(quin)_2(Him)_2]$	2.293(4)–2.418(4)	2.014(3)–2.052(3)	2.088(4)–2.135(4)	[52]
[Zn(Mepa)(quin)]	2.220(4)	2.015(2)	/ [2]	[53]
$[Zn(quin)_2(H_2O)]$ [1]	2.144(4), 2.147(4)	2.017(4), 1.994(4)	1.986(3)	[54]

[1] The complex has no inherent crystallographic symmetry. Two sets of zinc-to-quinaldinate bond distances are given thereby. [2] Not relevant to this study.

Surprisingly, in spite of the commercial availability of pyridine-based ligands, their zinc complexes with the exception of pyridine itself and nicotinamide are extremely rare. The scarce zinc(II) complexes with the enol form of 3-hydroxypyridine serving as a ligand invariably display coordination through a nitrogen atom. A single 3-Py-OH ligand in a penta-coordinated zinc(II) complex with the $[Zn(C_4H_8NOS_2)_2(3\text{-Py-OH})]$ composition (where $C_4H_8NOS_2^-$ denotes *N*-(2-hydroxyethyl)-*N*-methyldithiocarbamate) is bound at a distance of 2.0375(16) Å [56]. A significantly shorter bond than the one determined for $[Zn(quin)_2(3\text{-Py-OH})_2]$ (**4**) is yet another manifestation of the influence of the number of ligands over the bonding pattern (see above). The keto form of 3-hydroxypyridine can also coordinate to zinc(II). In $[Zn_2(N_3)_4(3\text{-Pyridone})]\cdot 2H_2O$, an azide complex with a two-dimensional layer structure, 3-pyridone is coordinated via an oxygen atom to two metal centers with Zn–O distances of 2.106(4) Å [57]. Furthermore, the literature reports on a zinc complex with the anionic form of 3-Py-OH, i.e., a 3-pyridinolato ion. 3-pyridinolate whose negative charge is localized on oxygen links a zinc porphyrin moiety with a boron subphthalocyanine [46]. The anion is coordinated to zinc via its pyridine nitrogen at a distance of 2.155(3) Å. Similar compounds are known also for 4-pyridinolato ion [46,47]. The title compound $[Zn(quin)_2(4\text{-Pyridone})]$ (**6**) bears more resemblance to $[ZnCl_2(4\text{-Pyridone})_2]$ [58]. In the latter, the coordination environment of the metal ion is tetrahedral with 4-pyridone ligands coordinated via O atoms at distances of 1.947 Å, distances which are very similar to the one in $[Zn(quin)_2(4\text{-Pyridone})]$ (**6**). The latter compound was obtained from the aqueous solution of zinc chloride and 4-Py-OH. *catena*-$[Zn_2(4\text{-Pyridone})(N_3)_4]\cdot H_2O$

exemplifies another binding mode of 4-pyridone: a μ_2-bridging coordination via oxygen with two distinctly different Zn–O distances, i.e., 2.1316(16) and 2.2106(15) Å [59]. It is pertinent to note that no complex of zinc(II) with the enol form of 4-Py-OH has been reported so far [34]. When binding to zinc(II), 3-hydroxymethylpyridine employs two coordination modes. A monodentate coordination via pyridine nitrogen was observed in a heptametallic zinc cluster with Zn–N distances of 2.042(3) Å [60], whereas a polymeric zinc complex with benzoate features a bidentate bridging coordination via both functional groups with Zn–N distance of 2.141(1) Å and Zn–O distance of 2.204(1) Å [61]. The corresponding bond in $[Zn(quin)_2(3\text{-}Hmpy)_2]$ (**5**) is longer. No other than a monodentate binding mode through pyridine nitrogen has been observed so far for 4-hydroxymethylpyridine. It is to be noted that the zinc-to-nitrogen bond length [2.021(2) Å] in a tetranuclear zinc phosphate [62] is also significantly shorter than in our complex $[Zn(quin)_2(4\text{-}Hmpy)_2]$ (**7**).

In contrast to other pyridine ligands used in this study, pyridine itself and 3,5-lutidine possess no functional groups that could participate in hydrogen-bonding interactions. Therefore only weak intermolecular interactions may be observed in the solid state structures of $[Zn(quin)_2(Py)_2]$ (**1**) and $[Zn(quin)_2(3,5\text{-}Lut)_2]$ (**2**). In the pyridine complex, C–H···O contacts, i.e., C(21)···O(2) $[-x, y + 0.5, -z + 0.5] = 3.101(4)$ and C(22)···O(2) $[-x, y + 0.5, -z + 0.5] = 3.106(5)$ Å, which occur between pyridine carbon atoms and a non-coordinated or *free* carboxylate oxygen link molecules into layers that are coplanar with the *bc* plane. The arrangement of complex molecules within layers is such that a $\pi\cdots\pi$ stacking interaction occurs between pairs of quinaldinate rings: a pyridine part of one quinaldinate makes a close approach to an arene part of another. With quinaldinate ligands two other types of $\pi\cdots\pi$ stacking interactions are possible: an interaction of two arene moieties or an interaction of two pyridine moieties. According to Janiak [63], there is a prevalent occurrence of pyridine···arene interactions. The relevant parameters of this interaction in **1** are: centroid–centroid distance = 3.593(2) Å, interplanar distance = 3.351(1) Å, dihedral angle = 1.5(1)°, and offset angle = 21.1° [63]. The connectivity pattern in the crystal structure of $[Zn(quin)_2(3,5\text{-}Lut)_2]$ (**2**) is different. The C–H···O contacts are of similar length, i.e., C(2)···O(2) $[-x + 3, -y + 1, -z] = 3.191(3)$ Å, but they occur between a quinaldinate C–H and a *free* carboxylate oxygen. They link molecules into infinite chains which are held together via various $\pi\cdots\pi$ stacking interactions occurring between aromatic rings and via T-shaped C–H$\cdots\pi$ interactions which occur between the 3,5-lutidine C–H and the arene part of quinaldinate (Table S2).

The solid state structures of other compounds are governed by stronger interactions. Following the general rule, all good hydrogen-bond donors and acceptors are engaged in hydrogen-bonding [64]. Hydrogen-bonding interactions are summed up in Table 4. For a complete list of weaker intermolecular interactions see Tables S1–S7. A well-known synthon [65] in supramolecular chemistry may be recognized in the structure of $[Zn(quin)_2(Nia)_2]\cdot 2CH_3CN$ (**3**), i.e., an amide···amide homosynthon with the N–H···O(carbonyl group) distance of 2.975(3) Å (Figure 5).

Table 4. Stronger intermolecular interactions in **3**–**7**.

Compound	Functions, Engaged in an Interaction [1]	Contact [Å] [2,3]
3	$NH_2\cdots COO^-$	N(3)···O(2) $[-x + 0.5, y + 0.5, -z + 0.5] = 2.885(3)$
4	$NH_2\cdots$C=O(amide)	N(3)···O(3) $[-x + 1, -y, -z + 1] = 2.975(3)$
	$OH\cdots COO^-$	O(3)···O(2) $[-x + 1.5, y - 0.5, -z + 1.5] = 2.640(2)$
5	$OH\cdots COO^-$	O(3)···O(2) $[x + 1, y + 1, z] = 2.697(2)$
6	NH(pyridone)$\cdots COO^-$	N(3)···O(22) $[x + 1.5, -y + 0.5, z - 0.5] = 2.783(2)$
	$COO^-\cdots COO^-$ [4]	O(11)···O(22) $[-x, -y + 1, -z + 1] = 2.934(2)$
7	$OH\cdots COO^-$	O(3)···O(2) $[-x + 1, -y, -z + 2] = 2.794(2)$

[1] If not stated otherwise, COO^- refers to a non-coordinated carboxylate oxygen atom. [2] For atom labels, see respective figures. [3] The distances may be compared to the corresponding sums of the van der Waals radii, 3.07 Å for N+O, and 3.04 Å for O+O [66]. [4] A short contact between a coordinated oxygen of one COO^- and a non-coordinated oxygen from another. See text.

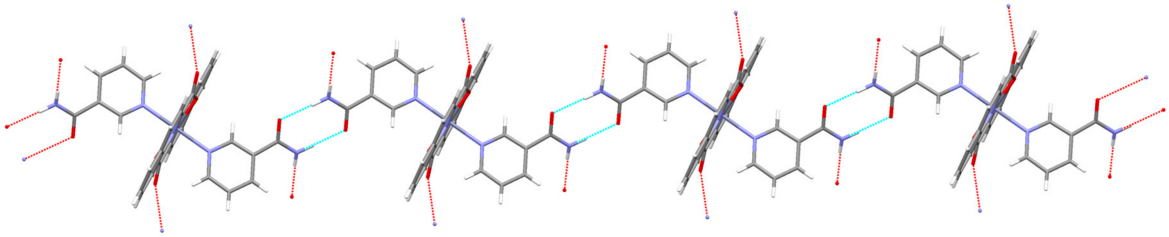

Figure 5. Section of a chain in $[Zn(quin)_2(Nia)_2]\cdot 2CH_3CN$ (**3**), highlighting the amide···amide homosynthon.

With each complex molecule containing two equivalent nicotinamide ligands, molecules are linked into chains. The amide-dimer motif has been conveniently designated as $R_2^2(8)$ [64]. The usually observed N–H···O contacts within the dimer are shorter, as exemplified by a co-crystal of 4-hydroxybenzamide/4,4′-bipyridine *N*,*N*′-dioxide with a distance of 2.892(3) Å [67]. The lengthening in **3** finds explanation in the involvement of the other NH_2 hydrogen atom in a hydrogen-bonding interaction with a non-coordinated carboxylate oxygen (shown in Figure 5 as a hanging dashed line) from an adjacent chain. Combination of both hydrogen-bonding motifs effectively links chains into layers which are coplanar with the [1 0 −1] plane (Figure 6). Each complex molecule within this layer forms altogether eight hydrogen bonds with its six closest neighbors. The layers interact via $\pi\cdots\pi$ stacking interactions with the shortest approach observed between the pyridine parts of the quinaldinate rings [centroid–centroid distance = 3.888(1) Å, interplanar distance = 3.4455(9) Å, dihedral angle = 0°, and offset angle = 27.6°]. According to Janiak [63], the latter are the least important among all three possible interactions for quinaldinate rings. The guest acetonitrile molecules are encapsulated between the layers.

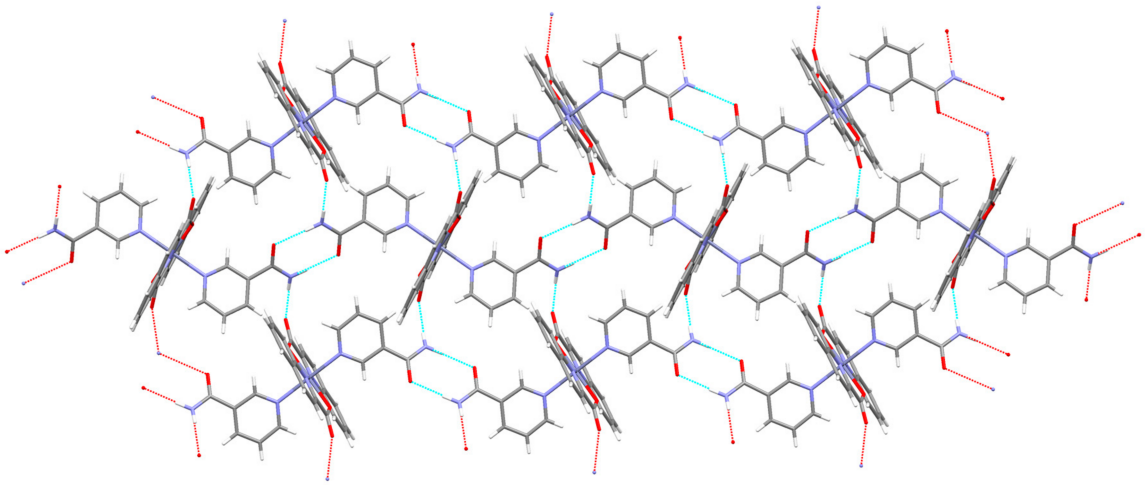

Figure 6. Section of a layer of $[Zn(quin)_2(Nia)_2]$ molecules, linked via N–H···O bonds.

The presence of a hydroxyl moiety in complex molecules of $[Zn(quin)_2(3\text{-Py-OH})_2]$ (**4**), $[Zn(quin)_2(3\text{-Hmpy})_2]$ (**5**), and $[Zn(quin)_2(4\text{-Hmpy})_2]$ (**7**) determines their connectivity in the solid state. In all structures, the hydroxyl moiety is engaged in a strong hydrogen bond with a non-coordinated carboxylate oxygen with the shortest bond occurring in **4**, a complex with 3-hydroxypyridine (Table 4). In **4**, each molecule forms four O–H···O interactions with four neighboring molecules. As a result, layers that are coplanar with the [1 0 −1] plane are formed (Figure 7).

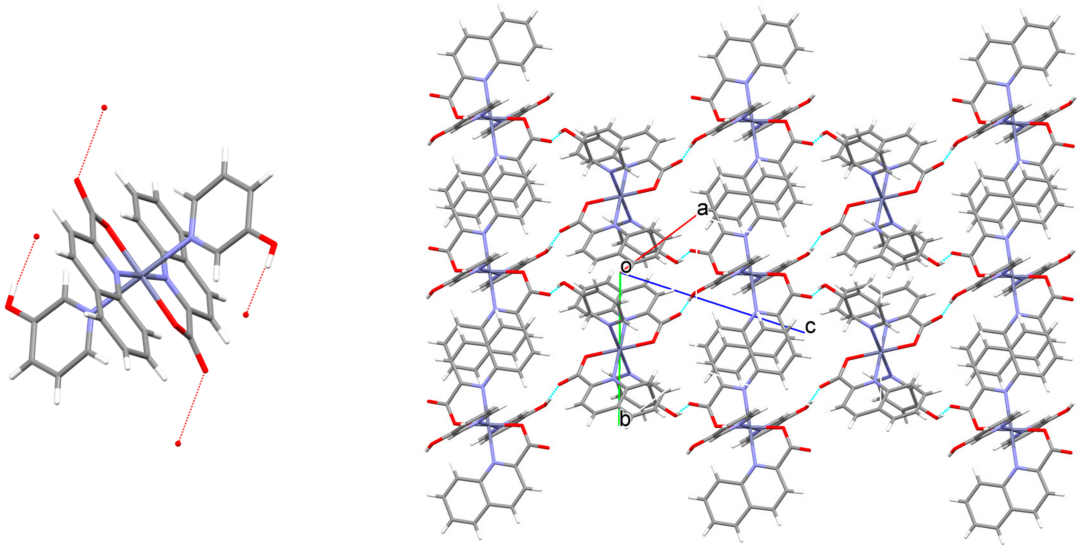

(**a**) (**b**)

Figure 7. Hydrogen-bonding pattern in $[Zn(quin)_2(3\text{-Py-OH})_2]$ (**4**). (**a**) Each complex molecule is engaged in four O–H···COO^- interactions. (**b**) Section of a layer.

A close proximity of molecules within layers allows $\pi\cdots\pi$ stacking interactions of quinaldinate rings and T-shaped C–H···π interactions between the quinaldinate C–H and the 3-Py-OH ring. The presence of a methylene group in 3-hydroxymethylpyridine makes the ligand more flexible when forming interactions with its surroundings. The O–H···O contact in $[Zn(quin)_2(3\text{-Hmpy})_2]$ (**5**) is slightly longer than in $[Zn(quin)_2(3\text{-Py-OH})_2]$ (**4**). The main difference between the pair is shown in the connectivity pattern. In the case of 3-Hmpy, each complex molecule forms four hydrogen bonds with two adjacent molecules producing an infinite chain pattern that extends along the 1 1 0 vector (Figure 8). A similar pattern is displayed by $[Zn(quin)_2(4\text{-Hmpy})_2]$ (**7**), a complex with 4-hydroxymethylpyridine with the longest O–H···O contact among all (Figure 9).

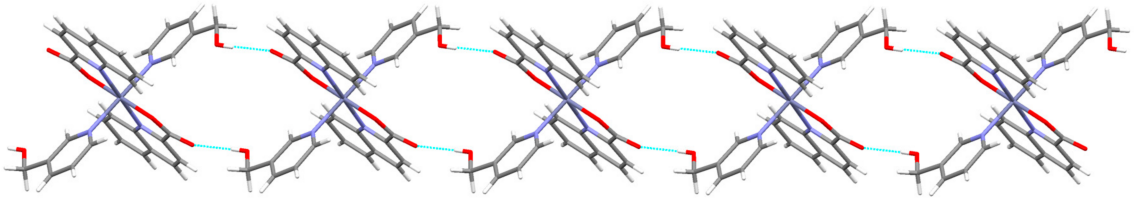

Figure 8. Hydrogen-bonding pattern in $[Zn(quin)_2(3\text{-Hmpy})_2]$ (**5**): a short section of a chain.

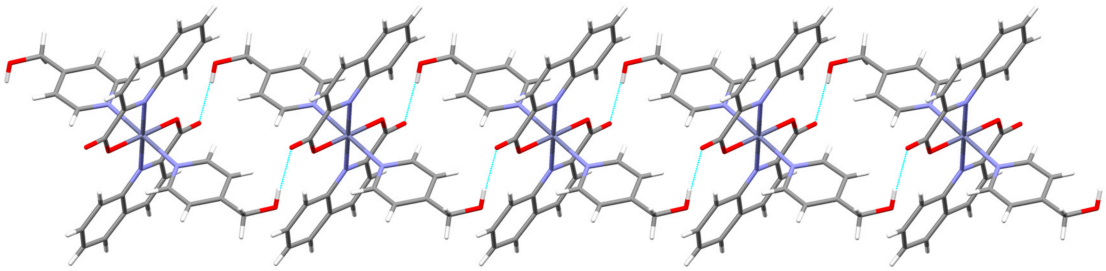

Figure 9. Hydrogen-bonding pattern in $[Zn(quin)_2(4\text{-Hmpy})_2]$ (**7**): a short section of a chain.

The packing of molecules in the structure of $[Zn(quin)_2(3\text{-Hmpy})_2]$ (**5**) is such that it allows $\pi\cdots\pi$ stacking interactions of 3-hydroxymethylpyridine rings [centroid–centroid distance = 4.297(1) Å, interplanar distance = 3.6011(8) Å, dihedral angle = 0°, and offset angle = 33.1°] and quinaldinate rings [an arene···arene type, centroid–centroid distance = 3.614(1) Å, interplanar distance = 3.4007(9) Å, dihedral angle = 0°, and offset angle = 19.8°]. A closer inspection of the packing of molecules in the structure of $[Zn(quin)_2(4\text{-Hmpy})_2]$ (**7**) reveals no $\pi\cdots\pi$ stacking interactions of 4-hydroxymethylpyridine rings. Instead, there is a T-shaped C–H$\cdots\pi$ interaction which occurs between the quinaldinate C–H and the 4-Hmpy ring. The $\pi\cdots\pi$ stacking interactions between quinaldinate rings may also be observed [a pyridine···arene type, centroid–centroid distance = 3.713(1) Å, interplanar distance = 3.3740(7) Å, dihedral angle = 1.4(1)°, and offset angle = 24.7°].

4-Pyridone of $[Zn(quin)_2(4\text{-Pyridone})]$ (**6**) is engaged via its NH group in hydrogen bonding interaction with COO^- of another molecule. Complex molecules are thereby linked into infinite chains (Figure 10). The packing arrangement of $[Zn(quin)_2(4\text{-Pyridone})]$ molecules allows another type of interaction: a dipole···dipole interaction between pairs of carbonyl moieties. Through the agency of the latter, dimeric entities are formed (illustrated in Figure 11). Within each dimer, all four carboxylates are involved. The carbonyl···carbonyl interactions are well-known [68]. They appear as three geometric motifs, differing in the number of short C···O contacts, i.e., distances that are significantly shorter than 3.6 Å. An antiparallel motif enables two short C···O contacts, as exemplified by a tertiary squaramide, bis-3,4-(diethylamino)-cyclobutene-1,2-dione, with lengths of 2.879 Å [69]. On the other hand, a sheared parallel and a perpendicular arrangement are characterized by one short contact [68]. In compound **6**, the shortest C···O contact [2.882(2) Å] occurs for a perpendicular arrangement of carbonyl moieties. The corresponding O···O contacts [2.934(2) Å] are shown in Figure 11 as dashed lines. Within this dimer an antiparallel alignment of a pair of carbonyl moieties may also be observed. It is characterized by two slightly longer C···O contacts [3.107(2) Å]. As a result of both the carbonyl···carbonyl interactions and the NH···COO^- hydrogen bonds, an infinite layered structure is formed (Figure 12).

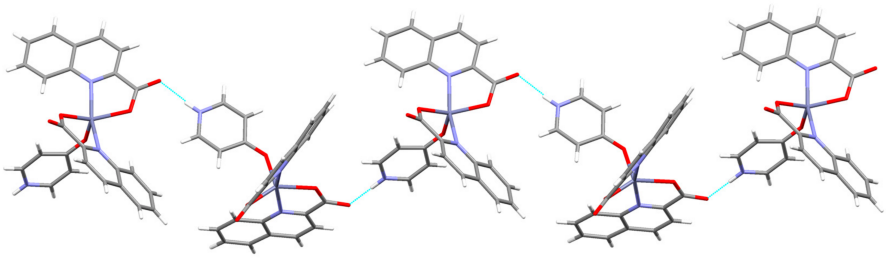

Figure 10. In $[Zn(quin)_2(4\text{-Pyridone})]$ (**6**), the N–H···COO^- interactions link molecules into chains.

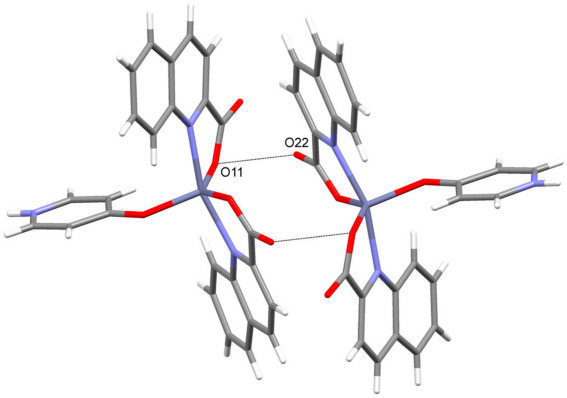

Figure 11. The carboxylate···carboxylate interactions in **6**.

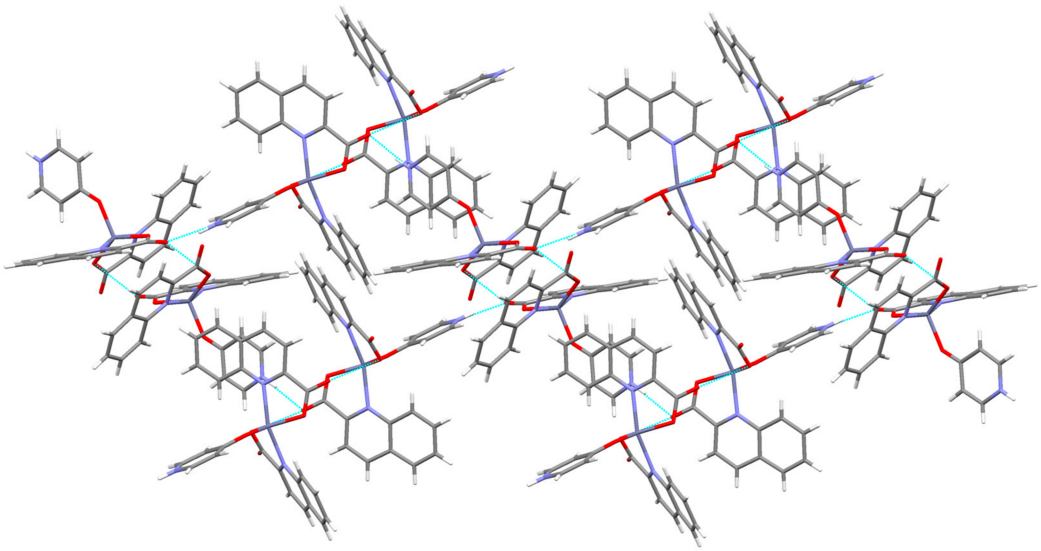

Figure 12. Linkage of [Zn(quin)$_2$(4-Pyridone)] molecules into layers in **6**.

3.3. Infrared Spectroscopy

The most relevant features of the infrared spectra of the title compounds concern the carbon–oxygen frequencies of the quinaldinato ligand and the characteristic absorptions of the pyridine-based ligands. The former are often used to diagnose the carboxylate binding mode [70,71]. In the case of a monodentate binding mode of the carboxylate, as in title compounds, a large difference in the positions of the ν_{asym}(COO) and ν_{sym}(COO) bands, known also as the splitting value Δ, may be observed. The title complexes display the splitting values Δ in the range 261–299 cm^{-1}. It is to be noted that values closer to 299 cm^{-1} were determined for [Zn(quin)$_2$(Py)$_2$] (**1**) and [Zn(quin)$_2$(3,5-Lut)$_2$] (**2**). Although in both compounds the *free* carboxylate oxygen participates in weak C–H···O interactions, the pair lacks stronger intermolecular interactions, i.e., hydrogen bonds. On the other hand, the spectra of the nicotinamide, 3-hydroxylmethylpyridine, 4-pyridone and 4-hydroxymethylpyridine complexes, where the carboxylate oxygen is engaged in hydrogen bonds, show values that are closer to 260 cm^{-1}. Our results are in line with the known influence of the strength of intermolecular interactions over the carboxylate splitting value Δ [52]. The positions of the ν_{asym}(COO) and ν_{sym}(COO) bands, i.e., 1654–1624 and 1368–1351 cm^{-1}, respectively, agree well with the data observed for related complexes, [Zn(quin)$_2$(1-methylimidazole)$_2$] [1642 and 1366 cm^{-1}] and [Zn(quin)$_2$(H$_2$O)] [1630 and 1390 cm^{-1}] [49,54].

Pyridine-based ligands, i.e., nicotinamide, 3-hydroxylmethylpyridine, and 4-hydroxymethy lpyridine, have functional groups that can be unambiguously identified by infrared spectroscopy [72]. A strong band at 1692 cm^{-1} in the spectrum of [Zn(quin)$_2$(Nia)$_2$]·2CH$_3$CN (**3**) may be assigned to the stretching vibration of the C=O moiety of the amide, whereas the absorptions due to the asymmetric and symmetric stretching vibrations of the NH$_2$ moiety occur as broad bands at 3292 and 3147 cm^{-1}. Absorptions of the alcohol C–O stretching vibrations appear in the spectra of [Zn(quin)$_2$(3-Hmpy)$_2$] (**5**) and [Zn(quin)$_2$(4-Hmpy)$_2$] (**7**) in the 1095–1010 cm^{-1} region. Two or three very intense bands may be observed. Their positions are like the ones found in the spectra of pure ligands. The ν(O–H) absorption of the hydroxymethylpyridine ligands may be seen in the spectra of [Zn(quin)$_2$(3-Hmpy)$_2$] (**5**) and [Zn(quin)$_2$(4-Hmpy)$_2$] (**7**) as a sharp, medium intensity band at 3367 or 3287 cm^{-1}, respectively. In the spectra of pure hydroxymethylpyridines this band is broad. A change of the shape of the ν(O–H) band in the spectra of complexes, as compared to that of pure ligands, results from a more organized hydrogen-bonding pattern involving the OH moiety in the solid state structures of complexes **5** and **7**, i.e., hydrogen bonds of the OH···COO$^-$ type and of moderate strength (Table 4). The absence of the ν(O–H) absorption in the spectrum of [Zn(quin)$_2$(4-Pyridone)] (**6**) confirms the keto form of the ligand.

3.4. Thermal Analysis of [Zn(quin)$_2$(Py)$_2$] (**1**), *[Zn(quin)$_2$(3,5-Lut)$_2$]* (**2**), *[Zn(quin)$_2$(3-Hmpy)$_2$]* (**5**), *[Zn(quin)$_2$(4-Hmpy)$_2$]* (**7**), *and [Zn(quin)$_2$(4-Pyridone)]* (**6**)

A pronounced similarity in the behavior of pyridine, 3,5-lutidine, 3- and 4-hydroxymethylpyridine complexes upon heating to 800 °C in argon was observed. In all, two well-resolved regions of major mass loss may be observed. Considering the higher volatility of pyridine-based ligands, the first step is due to their liberation from the zinc(II) coordination sphere, whereas the second one is governed by the pyrolysis of quinaldinate with the subsequent formation of zinc oxide. It is to be noted that the thermal stability of pyridine and 3,5-lutidine complexes is very similar. As will be shown, their decomposition starts at a 20–30 °C lower temperature than in other complexes. A narrower thermal stability window of the pair can be traced to the strength of intermolecular interactions in their solid state structures. The thermogravimetric (TG) curve of the pyridine complex, [Zn(quin)$_2$(Py)$_2$] (**1**), is shown in Figure 13, the TG curves of other compounds are given in Supplementary Materials. The first decomposition process of **1** starts at 155 °C and continues up to 230 °C. The accompanying mass loss is in excellent agreement with the release of pyridine ligands, calcd./found: 27.86%/27.90%. The residue {Zn(quin)$_2$} is stable until about 360 °C which marks the onset of the second decomposition process. The latter lasts up to ca. 570 °C and brings about a 49.12% decrease in mass. As shown by the differential scanning calorimetry (DSC) curve, both processes are endothermic. The final residual represents 28.97% of the initial mass. As confirmed by the powder X-ray diffraction, the resulting grey solid is a mixture of zinc oxide (calcd. 14.33%) with an amorphous material. The liberation of 3,5-lutidine ligands starts at 165 °C and continues up to 260 °C, calcd./found: 34.34%/34.31%. The second decomposition process occurs in the 330–500 °C interval with the 36.97% loss. The decomposition of the 4-Hmpy complex **7** starts at a slightly higher temperature, ca. 195 °C, and lasts up to 295 °C with the observed loss differing from the theoretical value for the release of 4-Hmpy molecules, calcd./found: 34.73%/29.16%. The first decomposition stage is immediately followed by the second which is completed at ca. 570 °C and is accompanied by the 39.91% mass loss. The TG curve of 3-Hmpy complex **5** reveals a small, yet a non-negligible reduction of mass, ca. 1–2%, in the 25–125 °C interval that is probably due to the solvent associated with the sample. The first major decomposition process in the 185–225 °C interval is followed by the second in the 230–290 °C interval with mass losses of 18.49% and 17.27%, respectively. Their sum is consistent with the liberation of 3-Hmpy molecules, calcd./found: 34.76%/35.76%. The final decomposition commences at 350 °C and lasts up to 570 °C. The inspection of thermal properties of [Zn(quin)$_2$(3-Hmpy)$_2$] (**5**) in the oxidizing atmosphere revealed a similar behavior with two major differences: (i) the onset of all processes is at lower temperatures, and (ii) the final decomposition stage is highly exothermic. A mass loss of 1.45% may be observed in the 80–125 °C interval, followed by a two-step dissociation of 3-Hmpy ligands in the 165–275 °C interval with the total loss amounting to 34.20%. The overall decomposition with the formation of zinc oxide starts at 290 °C and is completed by 490 °C, calcd./found: 12.96%/12.38%.

The TG curve of [Zn(quin)$_2$(4-Pyridone)] (**6**), obtained in argon atmosphere, differs from other studied compounds. It shows three distinct regions of mass loss. The first one is completed by 140 °C and accounts for ca. 7.5% of the initial mass. It may be ascribed to the solvent content, present in the sample. The latter could not be verified from the analytical data. The second one in the 215–335 °C interval is due to the 4-pyridone elimination, calcd./found: 18.84%/19.37%. The last one commences at 340 °C. The degradation of the compound continues at higher temperature without completion.

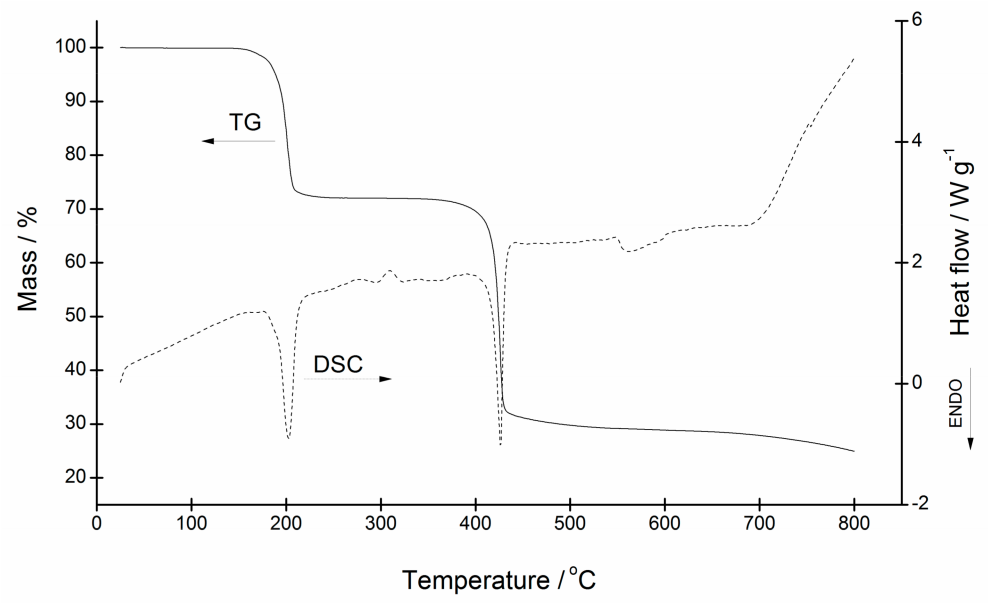

Figure 13. Thermogravimetric (TG) and differential scanning calorimetry (DSC) curves for $[Zn(quin)_2(Py)_2]$ (**1**).

4. Conclusions

Structural chemistry of a series of heteroleptic zinc(II) complexes with quinaldinate and pyridine-based ligands is presented. Complexes displayed two stoichiometries: (i) $[Zn(quin)_2L_2]$ (L = Py, 3,5-Lut, Nia, 3-Py-OH, 3-Hmpy and 4-Hmpy) with a nearly octahedral distribution of N_4O_2 donor sites, and $[Zn(quin)_2$(4-Pyridone)] with a square-pyramidal distribution of N_2O_3 donor sites. In all but a 4-hydroxypyridine compound, the pyridine-based ligand coordinated to the metal ion via its ring nitrogen atom. In the case of 4-Py-OH, its keto tautomeric form coordinated via an oxygen atom. Solid state structures of compounds displayed typical patterns of connectivity, determined by substituents of the pyridine-based ligands. For example, in $[Zn(quin)_2(Nia)_2]\cdot 2CH_3CN$ (**3**) the predicted structure directing role of amide was realized through the formation of the amide···amide homosynthon. On the other hand, the OH moieties in the 3-Py-OH, 3-Hmpy and 4-Hmpy complexes invariably formed hydrogen bonds to the carboxylate.

For pyridine ligands containing the $–CH_2OH$ functional group, new perspectives are opened with the introduction of a strong base to the system. Their anionic forms with the alkoxide oxygen atoms are known to engage both donor sites in coordination and could as such interfere with the structural integrity of the $\{Zn(quin)_2\}$ core. This remains to be investigated in our future studies.

Supplementary Materials: The following are available online at www.mdpi.com/2073-4352/8/1/52/s1, ORTEP diagrams of **2** (Figure S1), **5** (Figure S2), and **7** (Figure S3). Packing diagrams of **1** (Figure S4), **2** (Figure S5), and **7** (Figure S6). Exhaustive lists of intermolecular interactions (Tables S1–S7). TG/DSC curves of **2** (Figure S7), **7** (Figure S8), **5** (Figure S9), **5** heated in the air (Figure S10), and **6** (Figure S11). Infrared spectra (Figures S12–S17). NMR spectra of DMSO-d_6 solutions of **5** (Figures S18 and S19) and **7** (Figures S20 and S21). CCDC- 1581372 (**1**), 1581373 (**2**), 1581374 (**3**), 1581375 (**4**), 1581376 (**5**), 1581377 (**6**), and 1581378 (**7**) contain the supplementary crystallographic data for this paper. These data can be obtained free of charge at http://www.ccdc.cam.ac.uk/conts/retrieving.html (or from the Cambridge Crystallographic Data Centre, 12 Union Road, Cambridge CB2 1EZ, UK; Fax: +44-1223-336033).

Acknowledgments: This work was supported by a grant from the Slovenian Ministry of Education, Science and Sport (Grant P1-0134). The author is grateful to Darko Dolenc, Janez Košmrlj, and Damijana Urankar for NMR measurements, to Romana Cerc Korošec for thermal analyses and to graduate students Valentina Brzuhalski and Daniela Mikic for testing the reproducibility of syntheses.

Author Contributions: Barbara Modec conceived and designed the experiments, carried out the syntheses, performed X-ray structure determinations and analyzed the results.

Conflicts of Interest: The author declares no conflict of interest.

References

1. Keilin, D.; Mann, T. Carbonic anhydrase. Purification and nature of the enzyme. *Biochem. J.* **1940**, *34*, 1163–1176. [CrossRef] [PubMed]
2. Christianson, D.W. The structural biology of zinc. *Adv. Prot. Chem.* **1991**, *42*, 281–335.
3. Aoki, S.; Kimura, E. Zinc hydrolases. In *Comprehensive Coordination Chemistry*; McCleverty, J.A., Meyer, T.J., Eds.; Elsevier: Amsterdam, Nederland, 2004; pp. 601–640.
4. Andreini, C.; Banci, L.; Bertini, I.; Rosato, A. Zinc through the three domains of life. *J. Proteome Res.* **2006**, *5*, 3173–3178. [CrossRef] [PubMed]
5. Vahrenkamp, H. Why does nature use zinc—A personal view. *Dalton Trans.* **2007**, 4751–4759. [CrossRef] [PubMed]
6. Sousa, S.F.; Lopes, A.B.; Fernandes, P.A.; Ramos, M.J. The zinc proteome: A tale of stability and functionality. *Dalton Trans.* **2009**, 7946–7956. [CrossRef] [PubMed]
7. Lipton, A.S.; Heck, R.W.; Ellis, P.D. Zinc solid-state NMR spectroscopy of human carbonic anhydrase: Implications for the enzymatic mechanism. *J. Am. Chem. Soc.* **2004**, *126*, 4735–4739. [CrossRef] [PubMed]
8. Auld, D.S. The ins and outs of biological zinc sites. *Biometals* **2009**, *22*, 141–148. [CrossRef] [PubMed]
9. Chasapis, C.T.; Loutsidou, A.C.; Spiliopoulou, C.A.; Stefanidou, M.E. Zinc and human health: An update. *Arch. Toxicol.* **2012**, *86*, 521–534. [CrossRef] [PubMed]
10. Tarushi, A.; Kljun, J.; Turel, I.; Pantazaki, A.A.; Psomas, G.; Kessissoglou, D.P. Zinc(II) complexes with the quinolone antibacterial drug flumequine: Structure, DNA- and albumin-binding. *New J. Chem.* **2013**, *37*, 342–355. [CrossRef]
11. Mjos, K.D.; Orvig, C. Metallodrugs in medicinal inorganic chemistry. *Chem. Rev.* **2014**, *114*, 4540–4563. [CrossRef] [PubMed]
12. Ni, L.; Wang, J.; Liu, C.; Fan, J.; Sun, Y.; Zhou, Z.; Diao, G. An asymmetric binuclear zinc(II) complex with mixed iminodiacetate and phenanthroline ligands: Synthesis, characterization, structural conversion and anticancer properties. *Inorg. Chem. Front.* **2016**, *3*, 959–968. [CrossRef]
13. Indoria, S.; Lobana, T.S.; Sood, H.; Arora, D.S.; Hundal, G.; Jasinski, J.P. Synthesis, spectroscopy, structures and antimicrobial activity of mixed-ligand zinc(II) complexes of 5-nitro-salicylaldehyde thiosemicarbazones. *New J. Chem.* **2016**, *40*, 3642–3653. [CrossRef]
14. Koleša-Dobravc, T.; Maejima, K.; Yoshikawa, Y.; Meden, A.; Yasui, H.; Perdih, F. Vanadium and zinc complexes of 5-cyanopicolinate and pyrazine derivatives: Synthesis, structural elucidation and in vitro insulin-mimetic activity study. *New. J. Chem.* **2017**, *41*, 735–746. [CrossRef]
15. McCall, K.; Huang, C.-C.; Fierke, C.A. Function and mechanism of zinc metalloenzymes. *J. Nutr.* **2000**, *130*, 1437S–1446S. [CrossRef] [PubMed]
16. Pearson, R.G. Hard and soft acids and bases. *J. Am. Chem. Soc.* **1963**, *85*, 3533–3539. [CrossRef]
17. Huheey, J.E.; Keller, E.A.; Keiter, R.L. *Inorganic Chemistry: Principles of Structure and Reactivity*, 4th ed.; Harper Collins College Publishers: New York, NY, USA, 1993; pp. 394–413, ISBN 0-06-042995-X.
18. Laitaoja, M.; Valjakka, J.; Janis, J. Zinc coordination spheres in protein structures. *Inorg. Chem.* **2013**, *52*, 10983–10991. [CrossRef] [PubMed]
19. Yao, S.; Flight, R.M.; Rouchka, E.C.; Moseley, H.N.B. A less-biased analysis of metalloproteins reveals novel zinc coordination geometries. *Proteins Struct. Funct. Genet.* **2015**, *83*, 1470–1487. [CrossRef] [PubMed]
20. Parkin, G. The bioinorganic chemistry of zinc: Synthetic analogues of zinc enzymes that feature tripodal ligands. *Chem. Commun.* **2000**, 1971–1985. [CrossRef]
21. Bosch, S.; Comba, P.; Gahan, L.R.; Schenk, G. Dinuclear zinc(II) complexes with hydrogen bond donors as structural and functional phosphatase models. *Inorg. Chem.* **2014**, *53*, 9036–9051. [CrossRef] [PubMed]
22. Linder, D.P.; Rodgers, K.R. Methanethiol binding strengths and deprotonation energies in Zn(II)-imidazole complexes from M05-2X and MP2 theories: Coordination number and geometry influences relevant to zinc enzymes. *J. Phys. Chem. B* **2015**, *119*, 12182–12192. [CrossRef] [PubMed]
23. Yoshikawa, Y.; Ueda, E.; Kawabe, K.; Miyake, H.; Takino, T.; Sakurai, H.; Kojima, Y. Development of new insulinomimetic zinc(II) picolinate complexes with a $Zn(N_2O_2)$ coordination mode: Structure characterization, in vitro, and in vivo studies. *J. Biol. Inorg. Chem.* **2002**, *7*, 68–73. [CrossRef] [PubMed]

24. Wang, Y.-T.; Fan, H.-H.; Wang, H.-Z.; Chen, X.-M. A solvothermally in situ generated mixed-ligand approach for NLO-active metal-organic framework materials. *Inorg. Chem.* **2005**, *44*, 4148–4150. [CrossRef] [PubMed]
25. Papatriantafyllopoulou, C.; Raptopoulou, C.P.; Terzis, A.; Janssens, J.F.; Manessi-Zoupa, E.; Perlepes, S.P.; Plakatouras, J.C. Assembly of a helical zinc(II) chain and a two-dimensional cadmium(II) coordination polymer using picolinate and sulfate anions as bridging ligands. *Polyhedron* **2007**, *26*, 4053–4064. [CrossRef]
26. Konidaris, K.F.; Polyzou, C.D.; Kostakis, G.E.; Tasiopoulos, A.J.; Roubeau, O.; Teat, S.J.; Manessi-Zoupa, E.; Powell, A.K.; Perlepes, S.P. Metal ion-assisted transformations of 2-pyridinealdoxime and hexafluorophosphate. *Dalton Trans.* **2012**, *41*, 2862–2865. [CrossRef] [PubMed]
27. Enthaler, S.; Wu, X.-F.; Weidauer, M.; Irran, E.; Döhlert, P. Exploring the coordination chemistry of 2-picolinic acid to zinc and application of the complexes in catalytic oxidation chemistry. *Inorg. Chem. Commun.* **2014**, *46*, 320–323. [CrossRef]
28. Mohammadnezhad, G.; Ghanbarpour, A.R.; Amini, M.M.; Ng, S.W. Bis(μ-quinoline-2-carboxylato)-$\kappa^3N,O:O;\kappa^3O:N,O$-bis[(acetato-$\kappa^2O,O'$)(methanol-$\kappa O$)lead(II)]. *Acta Cryst.* **2010**, *E66*, m963. [CrossRef] [PubMed]
29. Zurowska, B.; Mrozinski, J.; Ciunik, Z. Structure and magnetic properties of a copper(II) compound with *syn-anti* carboxylato- and linear Cu–Cl–Cu chloro-bridges. *Polyhedron* **2007**, *26*, 3085–3091. [CrossRef]
30. Zurowska, B.; Slepokura, K. Structure and magnetic properties of polynuclear copper(II) compounds with *syn-anti* carboxylato- and bromo-bridges. *Inorg. Chim. Acta* **2008**, *361*, 1213–1221. [CrossRef]
31. Chowdhury, A.D.; De, P.; Mobin, S.M.; Lahiri, G.K. Influence of nitrosyl coordination on the binding mode of quinaldate in selective ruthenium frameworks. Electronic structure and reactivity aspects. *RSC Adv.* **2012**, *2*, 3437–3446. [CrossRef]
32. Starynowicz, P. Structure of bis-μ-(2-quinolinecarboxylato-*O*,*O*,*O*′)bis[triaqua(2-quinolinecarboxylato-*N*,*O*)(2-quinolinecarboxylato-*O*)neodymium(III)] trihydrate. *Acta Cryst.* **1990**, *C46*, 2068–2070. [CrossRef]
33. Groom, C.R.; Bruno, I.J.; Lightfoot, M.P.; Ward, S.C. The Cambridge Structural Database. *Acta Cryst.* **2016**, *B72*, 171–179. [CrossRef] [PubMed]
34. Coxall, R.A.; Harris, S.G.; Henderson, D.K.; Parsons, S.; Tasker, P.A.; Winpenny, R.E.P. Inter-ligand reactions: In situ formation of new polydentate ligands. *J. Chem. Soc. Dalton Trans.* **2000**, 2349–2356. [CrossRef]
35. Yue, Z.-Y.; Cheng, C.; Gao, P.; Yan, P.-F. *Trans*-Bis(methanol-κO)bis(2-quinoline-carboxylato-κ^2N,O)zinc(II). *Acta Cryst.* **2004**, *E60*, m82–m84.
36. Williams, D.B.G.; Lawton, M. Drying of organic solvents: Quantitative evaluation of the efficiency of several desiccants. *J. Org. Chem.* **2010**, *751*, 8351–8354. [CrossRef] [PubMed]
37. Zhang, W.Z.; Shuang, M.; Zhu, M.C.; Lei, L.; Gao, E.J. Synthesis, crystal structure, and photoluminescence of zinc complex $[Zn(Qina)_2(DMSO)_2]\cdot 2DMSO$. *Russ. J. Coord. Chem.* **2009**, *35*, 874–879. [CrossRef]
38. *CrysAlis PRO*, Version 1.171.35.11; Agilent Technologies: Yarnton, Oxfordshire, UK, 2011.
39. Sheldrick, G.M. A short history of SHELX. *Acta Cryst.* **2008**, *A64*, 112–122. [CrossRef] [PubMed]
40. Sheldrick, G.M. Crystal structure refinement with SHELXL. *Acta Cryst.* **2015**, *C71*, 3–8.
41. Farrugia, J.J. ORTEP-3 for Windows—A version of ORTEP-III with a graphical user interface (GUI). *J. Appl. Crystallogr.* **1997**, *30*, 565. [CrossRef]
42. Macrae, C.F.; Edgington, P.R.; McCabe, P.; Pidcock, E.; Shields, G.P.; Taylor, R.; Towler, M.; van de Streek, J. Mercury: Visualization and analysis of crystal structures. *J. Appl. Cryst.* **2006**, *39*, 453–457. [CrossRef]
43. *CrystalMaker for Windows*, Version 2.6.1; CrystalMaker Software, Ltd.: Oxfordshire, UK, 2007.
44. Katritzky, A.R.; Lagowski, J.M. Prototropic tautomerism of heteroaromatic compounds: I. General discussion and methods of study. *Adv. Heterocycl. Chem.* **1963**, *1*, 311–338.
45. Rawson, J.M.; Winpenny, R.E.P. The coordination chemistry of 2-pyridone and its derivatives. *Coord. Chem. Rev.* **1995**, *139*, 313–374. [CrossRef]
46. Xu, H.; Ng, D.K.P. Construction of subphthalocyanine-porphyrin and subphthalocyanine heterodyads through axial coordination. *Inorg. Chem.* **2008**, *47*, 7921–7927. [CrossRef] [PubMed]
47. Choi, M.T.M.; Choi, C.-F.; Ng, D.K.P. Assembling tetrapyrole derivatives through axial coordination. *Tetrahedron* **2004**, *60*, 6889–6894. [CrossRef]
48. Koval'chukova, O.V.; Strashnova, S.B.; Zaitsev, B.E.; Vovk, T.V. Synthesis and physicochemical properties of some transition metal complexes with 3-hydroxypyridine. *Russ. J. Coord. Chem.* **2002**, *28*, 767–770. [CrossRef]
49. Zevaco, T.A.; Görls, H.; Dinjus, E. Synthesis, spectral and structural characterization of zinc carboxylate $[Zn(2\text{-quinolinecarboxylato})_2(1\text{-methylimidazole})_2]$. *Inorg. Chim. Acta* **1998**, *269*, 283–286. [CrossRef]

50. Braga, D.; Grepioni, F.; Tedesco, E.; Biradha, K.; Desiraju, G.R. Hydrogen bonding in organometallic crystals. 6. X–H···M hydrogen bonds and M···(H–X) pseudo-agostic bonds. *Organometallics* **1997**, *16*, 1846–1856. [CrossRef]
51. Brookhart, M.; Green, M.L.H.; Parkin, G. Agostic interactions in transition metal compounds. *Proc. Natl. Acad. Sci. USA* **2007**, *104*, 6908–6914. [CrossRef] [PubMed]
52. Dobrzynska, D.; Lis, T.; Jerzykiewicz, L.B. 3D supramolecular network constructed by intermolecular interactions in mixed ligand complex of zinc. *Inorg. Chem. Commun.* **2005**, *8*, 1090–1093. [CrossRef]
53. Brand, U.; Vahrenkamp, H. A new tridentate *N*,*N*,*S* ligand and its zinc complexes. *Inorg. Chem.* **1995**, *34*, 3285–3293. [CrossRef]
54. Okabe, N.; Muranishi, Y. Aquabis(quinoline-2-carboxylato-κ^2N,*O*)zinc(II). *Acta Cryst.* **2003**, *E59*, m244–m246. [CrossRef]
55. Addison, A.W.; Rao, T.N.; Redijk, J.; van Rijn, J.; Verschoor, G.C. Synthesis, structure, and spectroscopic properties of copper(II) compounds containing nitrogen-sulphur donor ligands: The crystal and molecular structure of aqua[1,7-bis(*N*-methylbenzimidazol-2′-yl)-2,6-dithiaheptane]copper(II) perchlorate (τ is calculated using the equation (β–α)/60 where α and β stand for basal angles. Its value is 0 for a perfect square pyramid, and it becomes unity for a trigonal bipyramid). *J. Chem. Soc. Dalton Trans.* **1984**, 1349–1356. [CrossRef]
56. Jotani, M.M.; Arman, H.D.; Poplaukhin, P.; Tiekink, E.R.T. Bis(*N*,*N*-diethyldithiocarbamato-κ^2S,*S*′)(3-hydroxy pyridine-κN)zinc and bis[*N*-(2-hydroxyethyl)-*N*-methyldithiocarbamato-κ^2S,*S*′](3-hydroxypyridine-κN)zinc: Crystal structures and Hirshfeld surface analysis. *Acta Cryst.* **2016**, *E72*, 1700–1709. [CrossRef] [PubMed]
57. Goher, M.A.S.; Sodin, B.; Bitschnau, B.; Fuchs, E.C.; Mautner, F.A. Ladders, rings and cubes as structural motifs in three new zinc(II) azide complexes: Synthesis, spectral and structural characterization. *Polyhedron* **2008**, *27*, 1423–1431. [CrossRef]
58. Masse, R.; Fur, Y.L. Crystal structure of bis(4-pyridone)dichlorozinc(II), $ZnCl_2(C_5H_5NO)_2$. *Zeitschrift für Kristallographie New Cryst. Struct.* **1998**, *213*, 114.
59. Mautner, F.A.; Berger, C.; Gspan, C.; Sudy, B.; Fisher, R.C.; Massoud, S.S. Pyridyl and triazole ligands directing the assembling of zinc(II) into coordination polymers with different dimensionality through azides. *Polyhedron* **2017**, *130*, 136–144. [CrossRef]
60. Feazell, R.P.; Carson, C.E.; Klausmeyer, K.K. Synthesis of a functionalized monomer of the rare $M_7O_2^{10+}$ double tetrahedron Zn cluster. *Inorg. Chem. Commun.* **2007**, *10*, 873–875. [CrossRef]
61. Zelenak, V.; Cisarova, I.; Sabo, M.; Llewellyn, P.; Gyoryova, K. A Zn(II)-coordination polymer formed by benzoate and 3-pyridinemethanol ligands: Synthesis, spectroscopic properties, crystal structure and kinetics of thermal decomposition. *J. Coord. Chem.* **2004**, *57*, 87–96.
62. Murugavel, R.; Kuppuswamy, S.; Boomishankar, R.; Steiner, A. Hierarchical structures built from a molecular zinc phosphate core. *Angew. Chem. Int. Ed.* **2006**, *45*, 5536–5540. [CrossRef] [PubMed]
63. Janiak, C. A critical account on π–π stacking in metal complexes with aromatic nitrogen-containing ligands. *J. Chem. Soc. Dalton Trans.* **2000**, *21*, 3885–3896. [CrossRef]
64. Etter, M.C. Encoding and decoding hydrogen-bond patterns of organic compounds. *Acc. Chem. Res.* **1990**, *23*, 120–126. [CrossRef]
65. Aakeröy, C.B.; Scott, B.M.T.; Smith, M.M.; Urbina, J.F.; Desper, J. Establishing amide···amide reliability and synthon transferability in the supramolecular assembly of metal-containing one-dimensional architectures. *Inorg. Chem.* **2009**, *48*, 4052–4061. [CrossRef] [PubMed]
66. Douglas, B.B.; McDaniel, D.H.; Alexander, J.J. *Concepts and Models of Inorganic Chemistry*, 3rd ed.; Wiley: New York, NY, USA, 1994; ISBN 978-0-471-62978-8.
67. Babu, N.J.; Reddy, L.S.; Nangia, A. Amide-*N*-oxide heterosynthon and amide dimer homosynthon in cocrystals of carboxamide drugs and pyridine *N*-oxides. *Mol. Pharm.* **2007**, *4*, 417–434. [CrossRef] [PubMed]
68. Allen, F.H.; Baalham, C.A.; Lommerse, J.P.M.; Raithby, P.R. Carbonyl-carbonyl interactions can be competitive with hydrogen bonds. *Acta Cryst.* **1998**, *B54*, 320–329. [CrossRef]
69. Prohens, R.; Portell, A.; Font-Bardia, M.; Bauza, A.; Frontera, A. Experimental and theoretical study of weak intermolecular interactions in crystalline tertiary squaramides. *CrystEngComm* **2016**, *18*, 6437–6443. [CrossRef]

70. Nakamoto, K. *Infrared and Raman Spectra of Inorganic and Coordination Compounds. Part B: Applications in Coordination, Organometallic, and Bioinorganic Chemistry*, 5th ed.; John Wiley & Sons, Inc.: New York, NY, USA, 1997; pp. 23–30, 57–62, ISBN 0-471-16392-9.
71. Deacon, G.B.; Phillips, R.J. Relationships between the carbon–oxygen stretching frequencies of carboxylato complexes and the type of carboxylate coordination. *Coord. Chem. Rev.* **1980**, *33*, 227–250. [CrossRef]
72. Colthup, N.B.; Daly, L.H.; Wiberley, S.E. *Introduction to Infrared and Raman Spectroscopy*; Academic Press International Edition: New York, NY, USA, 1964; pp. 263, 274.